A COST-EFFICIENT PREDICTIVE METHOD FOR AERODYNAMIC PERFORMANCE DEGRADATION OF HORIZONTAL TAIL UNDER ICING CONDITIONS

Salvatore Corcione¹, Agostino De Marco² & Vincenzo Cusati³

- ¹Assistant Professor of Flight Mechanics, University of Naples Federico II, Dept. of Industrial Engineering, salvatore.corcione@unina.it
- Associate professor, University of Naples Federico II, Dept. of Industrial Engineering, agodemar@unina.it
 Assistant Professor of Flight Mechanics, University of Naples Federico II, Dept. of Industrial Engineering, vincenzo.cusati@unina.it

Abstract

This study aims to develop a low-computational-cost methodology using a 2.5D aerodynamic approach to predict the effects of icing on swept lifting surfaces with varying levels of accuracy. The objective is to enable the integration of icing impact on aerodynamics within the aircraft's multi-disciplinary optimization workflow using a cost-effective and reliable predictive method. The developed approach utilizes well-established 2D inviscid methods to predict the shapes of iced airfoils across a wide range of airspeeds, angles of attack, liquid water content, droplet diameters, and temperatures. This collection of clean and iced geometries is examined through high-fidelity CFD simulations to produce aerodynamic data organized into a multidimensional database, which serves as a data source for a nonlinear vortex lattice method. The vortex lattice tool is utilized to estimate the 3D aerodynamic characteristics of various swept lifting surfaces, assessing the influence of the planform geometry on ice accretion and aerodynamics. By collecting the 3D results, a prediction method is developed to create a response surface for quickly estimating icing effects in terms of degradation of the key aerodynamic characteristics of a tailplane. Both 2D and quasi-3D results are compared to relevant experimental and high-fidelity numerical test cases to evaluate the reliability, accuracy, and limitations of the proposed approach in terms of ice shapes and aerodynamic characteristics.

Keywords: In-flight icing, Ice induced- aerodynamics decay, aircraft design

1. Introduction

Icing is one of the major causes of flight accidents posing substantial risks to aviation safety [1]. Because of ice accretion on aircraft surfaces, lift decreases and drag increases leading to a degradation of aircraft aerodynamic performance and controllability [2]. Aircraft icing influences flight safety in many ways. Under icing conditions, the aircraft experiences a reduction in the maximum lift coefficient and a decrease in the slope of the lift curve. Simultaneously, there is an increase in drag and the critical stall speed. If the pilot fails to monitor changes in airspeed and climb rate, the aircraft may approach the stall boundary [3, 4, 5, 6, 7, 8]. Icing on the wings can result in a reduction of the airfoil stall angle of attack, while tailplane icing, particularly in flap downwash flows, may induce a tailplane stall. These conditions can trigger pitch instability and, ultimately, result in a crash. Asymmetric icing can lead to additional rolling moments imposing limitations on lateral control or resulting in rolling and overturn [9]. Icing has adverse effects on control efficiency [10]. Flight tests demonstrate that tailplane icing can result in significantly increased stick force, reaching hundreds of pounds, making manipulation more challenging. Icing on the rudder's movable structure can lead to stuck rudder surfaces, rendering the aircraft uncontrollable. Additionally, icing on the leading edge of flaps causes premature air separation, reducing flap efficiency. Active de-icing or anti-ice systems are commonly utilized for aircraft main wings due to their crucial role in providing the majority of the aircraft lift.

These systems are employed to prevent potential catastrophic aerodynamic performance degradation. However, when it comes to aircraft tailplanes, the conventional strategy in aircraft design is to accept the presence of ice phenomena. This approach aims to minimize factors such as weight, costs, maintenance, and energy expenses. Consequently, this strategy results in an oversizing of the tailplanes. Essentially, while active measures are often taken for main wings, a more passive coexistence strategy is typically adopted for tailplanes to optimize various design considerations. Oversizing may result in unnecessary additional weight, parasitic drag, and increased fuel consumption for all flight conditions. Achieving more accurate sizing requires a thorough understanding of potential in-flight ice accretion and its impact on aerodynamic performance. Currently, in addition to on-site observations, analysis of in-flight icing is primarily conducted through icing wind tunnel experiments and in-flight icing simulations. However, both in-situ and icing wind tunnel experiments require a significant amount of labor and lack flexibility in investigation. In contrast, simulating in-flight icing provides a more efficient and flexible method for analyzing icing, offering the potential for a more comprehensive examination of this phenomenon in aircraft design. The state-of-the-art in numerical ice accretion relies on 3D solvers of Reynolds Averaged Navier-Stokes equations [11, 12, 13, 14]. These tools have a high computational cost advising against a step-by step ice simulation within aircraft optimization loops. Several approaches are available to reduce icing computational costs [15, 16, 17, 18]. Most of these works focus on developing methods to reduce the computational costs of predicting the ice shape over 2D airfoils and estimating the decay of the aerodynamic characteristics. None of these approaches has been systematically exploited to develop a prediction method for the aerodynamic performance under icing conditions of a generalized 3D aircraft empennage.

This work leverages a mixed fidelity tool to drastically cut the computational cost of ice shapes prediction and aerodynamic estimation, unlocking the possibility to explore a wide design space of tailplane shapes and icing conditions [19]. The collected data will be used to develop a prediction method in the form of a response surface, which will estimate the degradation in performance of iced tailplanes. The ultimate objective is to reduce the time required for predicting reliable 3D ice shapes and aerodynamic performance, and to develop a rapid and dependable prediction method for integration into a step-by-step aircraft optimization process, thereby overcoming the bottleneck caused by ice accretion in the multi-disciplinary workflow.

The rest of this paper is organized as follows. Section 2 provides a brief description of the ice accretion phenomena, a comprehensive description of the key physics aspects governing the problem, the description of the adopted methodology and a benchmarking with relevant experimental and numerical data in terms of ice shapes (both 2D and 3D). Section 3 illustrates the achieved results, some application studies and the analysis of the computation costs. Finally conclusions and final remarks are presented in Section 4.

2. Materials and Methods

Ice accumulation on aircraft poses a severe threat to flight safety, modifying aerodynamic surfaces and altering forces and moments influencing the aircraft's flight. Two main phenomena are ground icing, occurring when moisture accumulates on cold aircraft surfaces while on the ground, and inflight icing, caused by freezing water droplets during flight. Ground icing reduces lift and increases drag, while tail contamination can lead to lift issues and block the tail-elevator gap, causing various flight challenges. In-flight icing, the focus here, results from supercooled water droplets colliding with aircraft surfaces in clouds, impacting aerodynamic performance. Factors influencing icing include Liquid Water Content (LWC), temperature (T), and droplet size. Icing severity and type depend on temperature, with the typical range from 0°C to -20°C and a cold limit at -40°C. Droplets in clouds are usually <50 μm, but larger Supercooled Large Droplets (SLD) of 50-500 μm pose a significant hazard. Considering the entire size range is crucial for certification, typically referenced by Mean Volume Diameter (MVD). For a fixed geometry, ice accretion is influenced by several key physical factors: the rate at which water droplets are intercepted by the solid body (e.g., the airfoil), known as the water droplet collection efficiency; the water content in the clouds; the speed of the body as it moves through the clouds; and the rate at which the incoming water freezes and forms an ice buildup. The impingement area is determined by the body surface where water droplets make contact, as defined by the trajectories of the droplets that are tangent to the body. Therefore, these

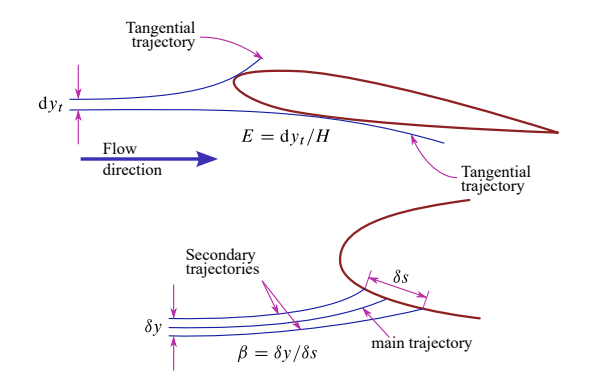


Figure 1 – Global and local collection efficiency.

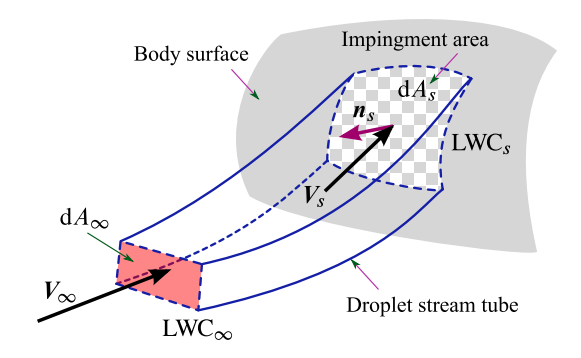


Figure 2 – Local catch efficiency 3D.

trajectories define the area of the body that comes into contact with water. Referring to Figure 1, it is possible to define the following:

• the global catch efficiency, *E*, which is the ratio between the upstream area formed by limiting trajectories and the area that they encompass on the body:

$$E = \frac{\mathrm{d}y_t}{H} \tag{1}$$

where dy_t represents the upstream area intercepted by limiting trajectories, and H represents the area intercepted on the body;

• the local collection efficiency, β . In a 2D flow field, the local collection efficiency refers to the ratio of the flow tube height, which is formed by the two limiting trajectories upstream, to its height on the body: $\delta y/\delta s$, where δy is the height intercepted upstream, and δs is the height obtained on the body.

In a 3D flow field, the local collection efficiency must be defined as the upstream area bounded by four trajectories and the area that they intercept on the body. Figure 2 illustrates the definitions of local catch efficiency in a 3D flow field. Assuming that the mass flow of water remains constant within a flow tube defined by two trajectories (four in a 3D flow field), with respect to the "i-th" surface element, the principle of mass conservation yields to the following definition of the collection efficiency:

$$\beta = \frac{dA_{\infty}}{dA_s} = \frac{\text{LWC}_s \left(-\vec{n}_s \cdot \vec{V}_s \right)}{\text{LWC}_{\infty} V_{\infty}} \tag{2}$$

Where LWC $_{\infty}$ represents the liquid water content upstream, V_{∞} denotes the freestream velocity and β refers to the local collection efficiency evaluated on the i-th surface element. This clearly highlights the correlation between the ice accretion and the LWC, the flow speed, the body shape and its attitude angle. Upon impinging on a solid body, droplets may partially or fully freeze based on the thermal balance. Airflow-body interaction enables heat dissipation through convection and heating from kinetic

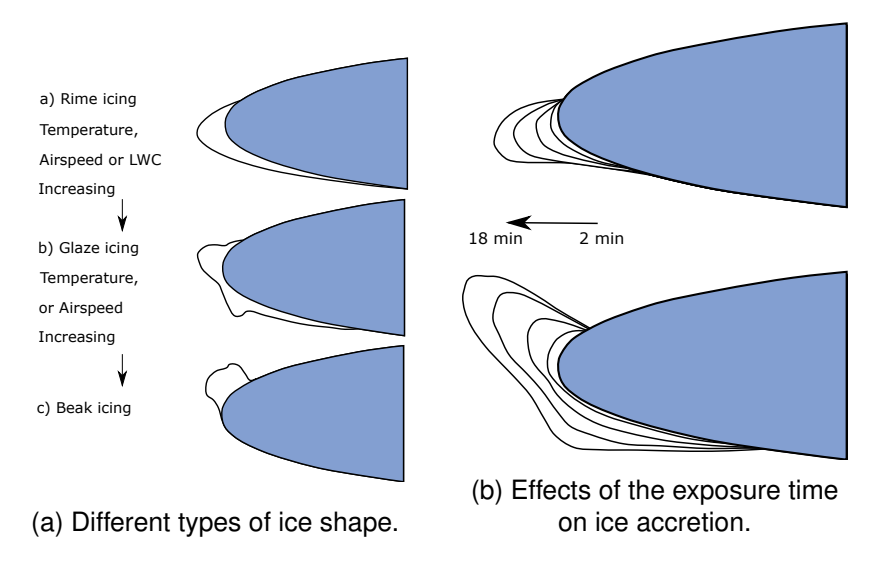


Figure 3 – Possible ice shapes and exposure time effects. Adapted from [20, 21].

energy impact. In low Liquid Water Content (LWC) and temperature conditions, forming ice stays below $0\,^{\circ}$ C, causing complete freezing. High LWC and slightly sub-zero air temperatures lead to partial instant freezing, with the remaining ice forming runback ice. Runback, caused by non-evaporative ice protection systems or large droplets, can create an ice ridge, posing a danger to aircraft performance. Two ice formations are identified: rime ice, resulting from supercooled droplets freezing on contact, characterized by a milky white appearance; and glaze ice, formed as water droplets flow over the aircraft surface, freezing away from the impact area. Glaze ice is transparent, with irregular shapes, often featuring one or two horns formed by freezing water running back. Figure 3a shows different types of ice accumulation [20]. Note that an increase in temperature, airspeed, or liquid water content (LWC) can cause a transition from rime icing to the more severe form of icing known as beak icing [20].

Various mixed ice shapes can occur in practice due to different ice accretion modes influenced by atmospheric conditions, freestream conditions, and aircraft parameters. Liquid water content (LWC) plays a crucial role in affecting both the rate and type of accretion. Higher LWC increases the likelihood of glaze ice formation. Mean Volume Diameter (MVD) influences the impingement area size, as larger droplets impact a larger surface. Airspeed has dual effects: increased convection and water mass flow rate lead to more ice accretion, but aerodynamic heating counters this by dissipating kinetic energy impact. Object geometry, such as airfoil shape, impacts ice formation. A decreased chord leads to higher catch efficiency and a faster ice formation rate. A larger chord, all else being equal, leads to less icing. Geometry also affects the wet area, while the duration of exposure to icing-promoting conditions influences ice buildup severity, with a constant wet area. Figure 3b illustrates the shapes of rime and glaze ice at four different exposure times. It is evident that the amount of ice accumulated on a surface increases with longer exposure time. Glaze ice accretions lead to an increase in horn size with prolonged exposure times.

By summarizing, the diameter of water droplets and aircraft geometry define the wetted area. The amount and shape of ice are determined by air temperature, aircraft geometry, velocity, liquid water content (LWC) in the air, and water droplet diameter (MVD).

2.1 2.5D Approach

The numerical simulation of the ice-accretion in order to compute the final iced shape could be approached in several ways. The state-of-the-art in numerical ice accretion relays on 3D solvers of Unsteady Reynolds Averaged Navier Stokes equations with multiphase flow physics crossing several steps to set-up and solve icing prediction through a full 3D URANS approach. Despite the high level of accuracy and increasing computational power, fully relying on computational fluid dynamics (CFD) still makes it prohibitive to integrate such an approach into a step-by-step aircraft Multi-Disciplinary Optimization process. In a recent paper, Page et al. [22] presented the results of the ice accretion

on a horizontal stabilizer of a jet transport aircraft calculated using the commercial software Ansys FENSAP-ICE to conduct state-of-the-art three-dimensional multishot in-flight icing simulations. Despite only the tail being affected by icing in the analysis, while the wing and the rest of the fuselage remained clean, the reported computational expense illustrates the extensive time required for the investigation of a 45 minutes holding flight condition in FAR 25 Appendix C cloud conditions. It took one week of wall clock time for the in-flight icing calculations, one day for the clean aerodynamic performance calculation, and another week for the calculation of the iced aerodynamics assessment, all utilizing 140 CPU processes.

This is the reason why this work aims to utilize a quasi-3D approach to significantly reduce the time needed to conduct thousands of simulations, with the goal of creating a method for predicting aerodynamic degradation in the form of a Response Surface Methodology (RSM).

Similar approaches have already been developed in past decades with reasonable results [23, 24]. Bragg [21] developed a quasi-3D algorithm to calculate the aerodynamic flow field by integrating a 3D vortex lattice code with a 2D viscous solver. Additionally, ice accumulations at various wing crosssections are calculated using a 2D droplet trajectory and the LEWICE inviscid icing code. Results for the clean aerodynamics and ice accretions were obtained on the 65%-scale Common Research Model aircraft and compared against high-fidelity computations using 3D RANS, as well as experimental data acquired at the NASA Glenn Icing Research Tunnel. The lift and drag results demonstrate reasonable agreement with the experiment, except in the vicinity of the stall region, and show comparable results to the 3D RANS computation for the case under study. The effects of loss of lift and increase in drag for the iced configurations investigated showed similar trends to those observed in the experiment. Hedde [24] developed a 3D icing model at ONERA by using Euler inviscid flow calculation, simulating droplet trajectories in a 3D grid, and remeshing the leading edge. The calculated 3D ice shapes were compared to experimental ones obtained on a non-rotating rotor blade tip, and the agreement was satisfactory. Then, the numerical results are compared to experimental shapes that exhibit scallop effects. The calculated shapes were significantly underestimated. The method has limitations in addressing complex three-dimensional aerodynamic effects, such as the aerodynamic interference between wing-body regions and the stall of clean and iced swept wings. These limitations arise from the assumption that the flow behaves in strips along the span, which lacks the necessary physics to accurately model these effects. Another limitation of the method is that the quality of the aerodynamic predictions is only as good as the 2D viscous solutions used in

To overcome the limitations in predicting the 2D aerodynamic data under clean and iced conditions, this paper modifies the previous approach by introducing a CFD-RANS solver to generate the required aerodynamic dataset to feed a non-linear Vortex Lattice Method (VLM). The proposed approach is basically a collection of several tools executing specific tasks, as depicted by the workflow of Figure 4.

The process starts by defining a reference lifting surface planform in terms of macro design parameters such as span (b), aspect ratio (\mathcal{R}), taper ratio (λ), planform area (S), and the sweep angle at the leading edge (Λ_{le}). In this work, the lifting surface is divided into several cross sections, with each section being associated to an airfoil. This set of 'dry' airfoils is then analyzed using a CFD-RANS solver, specifically Simcenter STAR-CCM+, under specific aerodynamic conditions (such as flight altitude, Mach number, and a range of angles of attack) to generate the required aerodynamic database for input into a nonlinear VLM code. The VLM is then executed to provide 3D data based on 2D, high-fidelity sectional data. Once the 'clean' lifting surface has been investigated, the icing calculation is then executed. That is, a 2D ice accretion prediction code is applied to each of the defined cross sections, taking into account local flow characteristics such as speed, effective incidence angles, and global thermodynamic parameters like the Liquid Water Content (LWC), median volume diameter (MVD), flight speed, and exposure time. Once the ice accretion step has been completed, each of the iced cross sections is reanalyzed using a RANS solver. The latter step provides the necessary aerodynamics in icing conditions. The iced dataset provides input for the VLM code to calculate 3D aerodynamics under icing conditions. Moreover, once the complete set of iced airfoils has been generated, a 3D CAD model of the lifting surface is produced. The process is then concluded

3D iced surface from 2.5D icing accretion approach 3D analysis, Nonlinear VLM Experimental database (i) VLM provides section-specific 2D viscous data 2D RANS information (airspeed, effective AoA) Surrogate mode Spanwise stations Local 2D, ice-off viscous data (ii) **2D ice accretion simulations** or a selected set of sections (iii) CAD geometry of iced surface is reconstructed 2D RANS Iced airfoil 2D Viscous data Surrogate model 3D analysis, Nonlinear VLM on 2.5D iced wing (iv.b) VLM computes iced-surface Iced airfoil local 2D viscous data $C_{L,H}$ Clean Ice-on Tail plane AoA sweep Iced 2.5D 7 Spanwise stations Tail plane lift coeff. Vs AoA

Figure 4 – Logical tree of the proposed 2.5D approach. Clean and Iced Aerodynamics.

by exporting all the necessary data related to clean and iced 3D aerodynamic characteristics.

2.2 2D Ice accretion approach

To drastically cut the time needed to fulfill the investigation of a wide range of configurations and conditions, a fast in-house developed code is used in this work to predict ice accretion on airfoils. The proposed approach is based on 2D inviscid methods to simulate the fluid, a Lagrangian formulation to predict droplets trajectories, a layer method [25] to evaluate the heat transfer, and a Messinger model is used to compute the local ice thickness [26] as well as the new ice shape. This one-way coupling process is repeated to simulate the desired exposure in a multi-step approach [13]. This procedure exhibits a satisfying level of accuracy with a reduced computational cost. In a nutshell, the ice accretion workflow implemented with the above-described technique follows these steps: (i) Calculating the trajectories of droplets and the local catch efficiency coefficient. (ii) Computing the heat transfer coefficient for a rough surface profile. (iii) Computing the thermodynamic balance that provides the rate of ice growth and the resulting ice shapes after a specified exposure time.

The trajectories are calculated using an explicit method that considers only the drag forces resulting from the velocity difference between the droplet and the surrounding flow field. The collection efficiency is evaluated by calculating the ratio of the mass flow. To take into account the roughness effects while estimating the heat transfer coefficient, the Makkonen correlation [27] is used. The roughness of the airfoil surface is estimated according to Shin et al. [28]. Messinger's equations [26] are used to calculate the local freezing fraction. Starting from the stagnation point the tool solves the steady heat balance equation for each consecutive facet, and then calculates the local equilibrium of the surface temperature, the freezing fraction and then the rate of icing. The unfrozen portion is then allowed to flow back to the nearby surface.

This code can also compute the 2D aerodynamic characteristics in both ice-on and ice-off conditions. However, the code considers the effects of compressibility but not those of viscosity.

Table 1 - 2D Experimental test cases conditions.

Conditions	CASE 241	CASE 242	CASE 251
MVD	30.0 µm	15.0 µm	21.5 µm
LWC	0.42g/m^3	0.81g/m^3	1.64g/m^3
Speed	103 m/s	$103 \mathrm{m/s}$	$103 \mathrm{m/s}$
Mach	0.31	0.31	0.31
Total temperature	−17.8 °C	-1.9 °C	−7.3 °C
Static temperature	−23.8 °C	−7.1 °C	−12.6 °C
Static pressure	92 528 Pa	92941 Pa	91 700 Pa
Chord	$0.4572\mathrm{m}$	$0.4572\mathrm{m}$	1.8288 m
Reynolds number	3.8×10^{6}	3.4×10^{6}	12.7×10^{6}
Spray time	5 min	5 min	6.63 min
Angle of attack	2 deg	2 deg	0 deg

2.3 Benchmark of 2D ice accretion

A reliable prediction of 2D ice shapes is the focal point on which the proposed 2.5D method is built. Thus, a validation of the proposed approach for estimating ice shapes under various conditions has been performed against several relevant experimental test cases. Here we show the results of three selected test cases from the AIAA Ice Prediction Workshop of 2021 [29], in particular, the test cases numbered 241, 242, and 251. These cases involve a NACA 23012 airfoil under various aerodynamic conditions. For instance, the boundary conditions of test case 241 should lead to rime ice formation, while the conditions of test case 242 should result in glaze ice accretion. Detailed information regarding the aerodynamic conditions under consideration is summarized in Table 1. Figure 5a, Figure 5b and Figure 5c illustrate the comparison between the experimental results (red dots) and the ice shape predicted by using the proposed approach (blue dots). These comparisons demonstrate a satisfactory agreement with the experimental results, even in predicting the complex shape of a glaze-ice case.

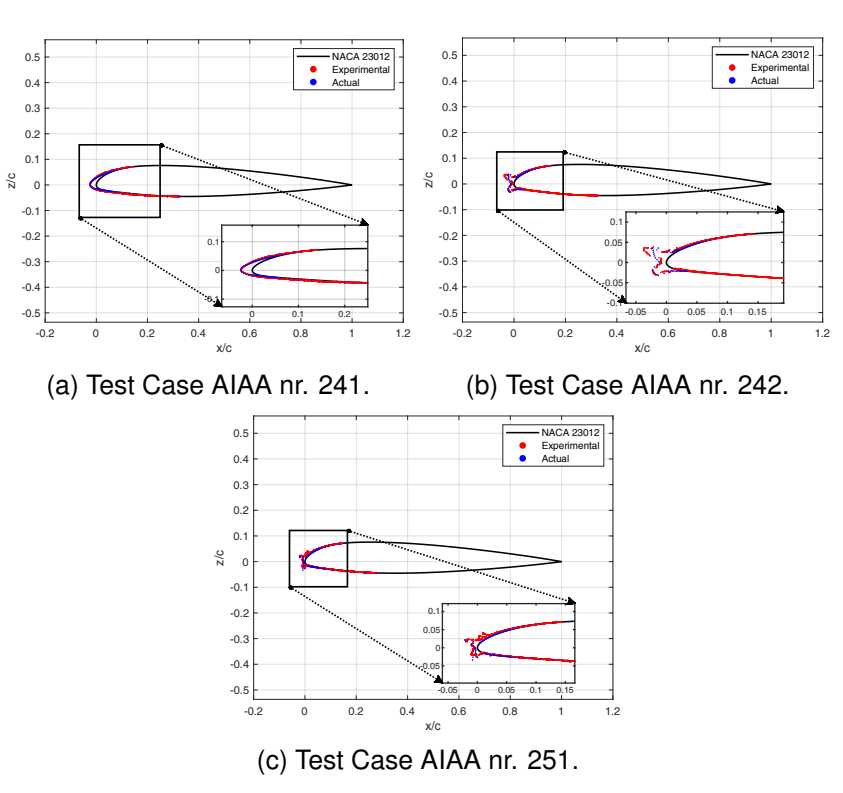


Figure 5 – Selected test cases for benchmarking the proposed 2D ice accretion approach.

Table 2 – 3D Experimental test cases conditions.

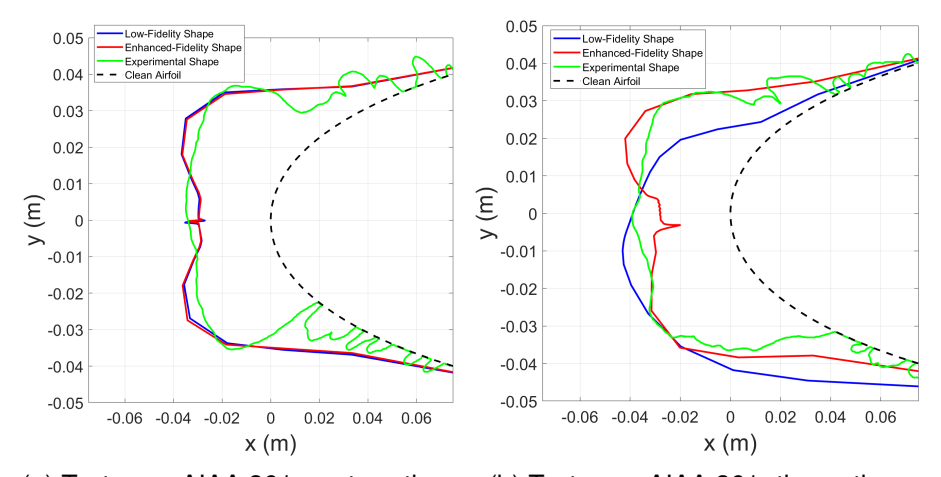
Parameter	CASE 361	CASE 362
MVD	34.70 µm	34.70 µm
LWC	0.50g/m^3	0.50g/m^3
Mach	0.32	0.32
Static temperature	257 K	266 K
Static pressure	92.321 Pa	92.321 Pa
Water density	$997.0 \mathrm{kg/m^3}$	$997.0 \mathrm{kg/m^3}$
Icing time	1200 s	1200 s
Angle of attack	0 deg	0 deg
Span	2.28 m	2.28 m
Sweep at leading edge	30 deg	30 deg
Airfoil	NACA 0012	NACA0012

2.3.1 Benchmark of the 2.5D approach

To evaluate the predictive capabilities for ice shapes produced by the application of the proposed 2.5D approach when a 3D swept wing is considered, some relevant experimental test cases have been selected to perform a comparison. In particular, the test cases AIAA-361 and AIAA-362 from the first AIAA ice prediction workshop database have been selected [29] to serve this purpose. All the information about the test conditions has been extracted from [29], and all the necessary data are summarized in Table 2, including the geometric features and icing conditions. Aiming at performing a 2.5D approach, the aerodynamics characteristics of five sections of the 3D wing under investigations have been extracted (specifically the sections located at 0.0, 25.0, 50.0, 75.0 and 100.0% of the wing span). These sections have been used to calculate the local ice shapes under the prescribed atmospheric conditions, see Table 2, and their resulting aerodynamic characteristics in clean and under icing conditions have been evaluated by means of CFD-RANS simulations in order to build up a CFD-based aerodynamic database compliant with the assigned airfoil, test-case geometries and aerodynamic conditions The comparison between the ice shapes at the root and tip section, provided by the experimental test cases, and the computed ones is shown in Figure 6 and Figure 7. The charts show three different curves, the green ones represent the experimental shapes, while the blue ones show the results in terms of ice shapes that can be obtained by means of 2.5D simulation when the aerodynamics of the sections is computed with the same 2D inviscid tool used for the ice accretion. Red curves show instead the ice shapes that can be obtained by a 2.5D simulation relying on 2D viscous database generated with CFD simulations. A more reliable aerodynamic dataset can provide more accurate local aerodynamics in terms of lift curve variation with respect to the local angle of attack. The latter gives more accurate feeds to the VLM tool, leading to local aerodynamic conditions closer to the experimental ones, this is reflected in the accuracy of the ice shapes that can be achieved by the proposed approach.

2.3.2 2D aerodynamics surrogate

Since the ultimate goal of this work is the development of a prediction method for the ice-dependent decay of aerodynamic characteristics of a generalized swept tailplane in the form of Response Surface Methodology (RSM), there is a need to analyze hundreds of cases under various icing conditions. In order to further reduce the computational cost of running a 2.5D approach involving 2D CFD-RANS simulations for various wing sections under different conditions, the 2D aerodynamics have been 'surrogated' by developing a dedicated database. A reference airfoil has been selected to serve as the standard cross-sectional profile for all tailplane planform designs under consideration. The chosen reference airfoil is the symmetrical four-digit NACA 0009, which is suitable for the tailplane of a transport jet aircraft. This airfoil has been investigated across a broad range of airspeeds, angles of attack, liquid water contents, droplet diameters, air temperatures, and chord lengths. This portfolio of clean and iced geometries has been investigated through high-fidelity, two-dimensional



- (a) Test case AIAA 361: root section. (b) Test case AIAA 361: tip section.
 - Figure 6 3D Ice shape prediction for test case AIAA 361.

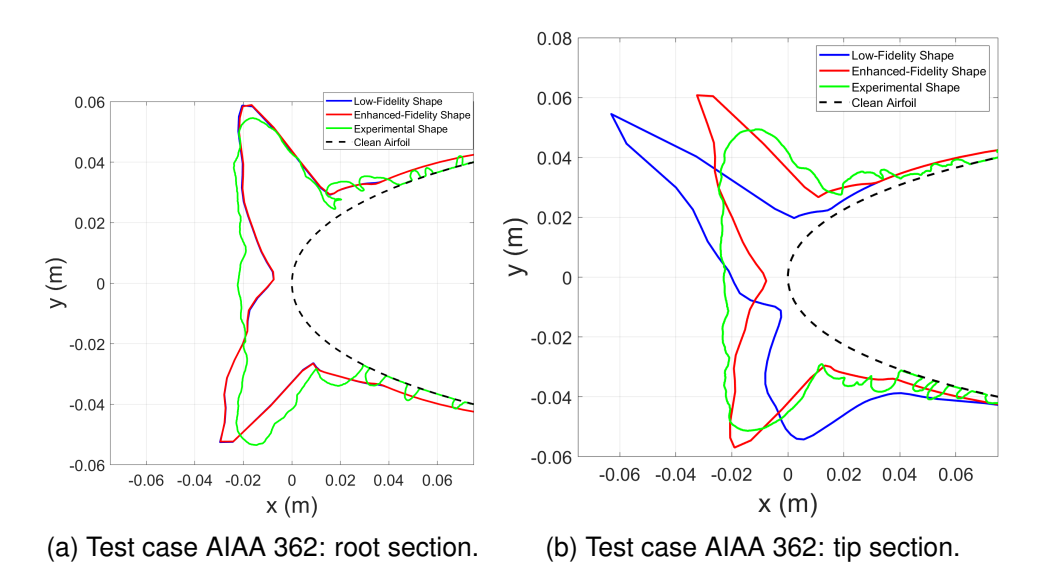


Figure 7 - 3D Ice shape prediction for test case AIAA 362.

computational fluid dynamics (CFD) simulations. The data produced has been organized into a multidimensional database, which serves as the data source for a nonlinear 3D Vortex Lattice Method (VLM) [30, 31].

Both ice-off and ice-on aerodynamics have been calculated using a steady Reynolds-Averaged Navier-Stokes (RANS) solver, specifically Simcenter STAR-CCM+. Preliminary mesh independence studies have been conducted to determine the optimal numerical set-up, with a primary focus on ice-on conditions.

The mesh domain consists of a rectangular region whose dimensions are related to the airfoil chord length. The domain extends 20 chords forward, upward, and downward from the leading edge, and 50 chords backward. The selected mesh type is an unstructured polygonal mesh, and a prism layer substrate is added to accurately simulate the boundary layers near the airfoil. Moreover, specific refinements have been added to enhance the prediction of flow fields. Detailed settings are specified in Table 3. The selected physics models include the steady flow model, coupled flow model with implicit integration and second-order discretization scheme, coupled energy model, ideal gas model, and Menter SST k- ω turbulent flow model.

To fulfill the mesh sensitivity study, a target iced airfoil has been selected form the available experimental test cases. The latter is the NACA0012 from the experimental study conducted by Shin and Bond at NASA Lewis Research Center [32]. Among the various test conditions, the selected condition

Table 3 – Mesh settings for the 2D airfoil.

Near field ref	inement controls
Mesh type	Unstructured polygonal mesh
Custom control type	Volumetric
Cells Size	2.5% of the base size
Airfoil refin	ement controls
Custom control type	Surface
Target surface size	0.25% of the base size
Minimum surface size	0.10% of the base size
Wing trailing edge	e refinement controls
Custom control type	Surface
Target surface size	0.10% of the base size
Minimum surface size	0.10% of the base size
Wake i	refinement
Custom control type	Wake region
Isotropic size	2.0% of base size
Growth rate	1.3
Prism la	yer controls
Number of prism layers	25
Near wall thickness	$3 \times 10^{-5} \mathrm{m}$
Prism layer total thickness	0.01 m

for conducting the mesh independence study includes the following operating parameters: an angle of attack of $4\,\mathrm{deg}$, a total temperature of $-5.56\,^\circ\mathrm{C}$, an airspeed of $102.82\,\mathrm{m/s}$, a LWC of $0.55\,\mathrm{g/m^3}$, a MVD of $20\,\mu\mathrm{m}$, and an ice accretion time of $7\,\mathrm{min}$.

Since the computational mesh has been parameterized with respect to a reference size, known as the "base size," the latter has been modified to facilitate the mesh sensitivity analysis. Different values of the base size include: 1.5 m, 1.2 m, 1.0 m, 0.7 m and 0.5 m. The number of cells corresponding to each mesh base size is reported in Table 4 along with the wall clock time required to perform 2000 iterations. The sensitivity study regarding the variation of aerodynamic coefficients with respect to the number of mesh cells is shown in Figure 9. The only experimental data available from the reference deals with the drag coefficient measurement. This data is reported as a dashed line on the chart of the drag coefficient in Figure 9a. The experimental drag coefficient is about 0.0311 (311 drag counts), while the CFD solution underestimates the drag providing for a value of approximately 0.0287 (287 drag counts). The estimated discrepancy is in line with similar estimates as reported by Shaw et al. [33], being lower 10%, this is a quite satisfactory estimate considering that the main goal of this work is to provide trends rather than absolute values of the aerodynamic performance decay due to icing. Perhaps matching the experimental drag with the CFD-RANS simulation is a non-trivial problem. Additionally, there is a discrepancy between the experimental ice shape and the predicted one, as depicted in Figure 8.

Considering the computational burden and the rate of change in the aerodynamic coefficients, it was determined that the best balance between computational time and accuracy is achieved with a mesh having a base size of $0.7\,\mathrm{m}$.

Once the numerical set-up has been established, a Design of Experiment (DoE) has been generated by varying all relevant parameters for ice accretion phenomena like air temperature, liquid water content, droplet mean volumetric diameter, Mach number, airfoil chord length and the angle of attack at which the ice shape is computed. Each point of the design space is analyzed over a wide range of angles of attack for both ice-off and ice-on conditions, specifically from -16° to 16° . Due to the high

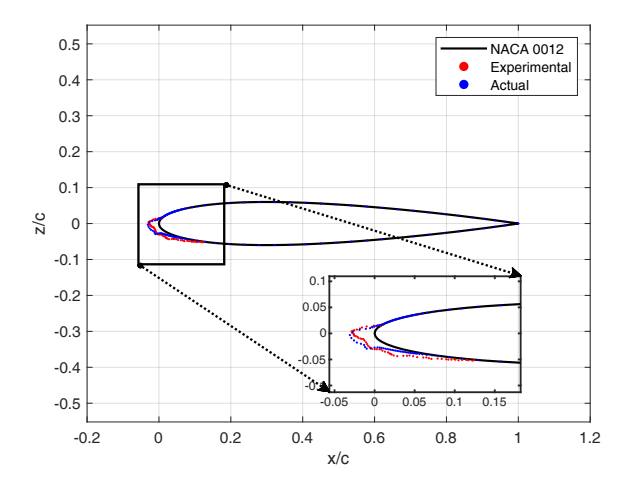


Figure 8 – 2D Ice shape prediction: NACA 0012, T = -5.56 °C, V = 102.82 m/s, Exposure time 7 min, LWC = 0.55 g/m³ and MVD = 20 µm [32] vs. proposed approach.

Table 4 – Number of cells per each tested base size and clock time per 2000 iterations.

Base Size (m)	Number of cell	Clock time (s) @6CPUs(3.60GHz)
1.5	6.97×10^{4}	3.02×10^{3}
1.2	9.28×10^{4}	4.47×10^{3}
1.0	1.41×10^{5}	7.18×10^{3}
0.7	2.24×10^{5}	1.04×10^{4}
0.5	4.36×10^{5}	2.01×10^{4}
0.3	1.05×10^6	5.07×10^4

number of costly numerical simulations, the design space has been generated by means of a Latin Hyper-Cube Sampling (LHCS) approach. LHCS is a method for generating a nearly random sample of parameter values from a multidimensional distribution [34, 35, 36], chosen to achieve maximum coverage of the design space with a reduced number of sample points.

Table 5 resumes all variables envisaged into the DoE and their lower and upper bounds. The values for the airfoil chord length is conceived to cover a wide spectrum of chord length distributions that could potentially represent the tailplane planform of a jet transport aircraft.

Regarding the atmospheric icing conditions, the range of the DoE has been established in accordance with Appendix C of 14 CFR Part 25 [37].

Appendix C provides two different charts representing two scenarios: "continuous maximum" and "intermittent maximum". These charts essentially show the probable maximum value of cloud water concentration (also known as the liquid water content, LWC) that is anticipated on average over a specific reference distance, based on the temperature and droplet size in the cloud. Generally, continuous maximum conditions are applied to the sizing of ice protection systems for large aircraft, while intermittent maximum conditions are applied to engine ice protection devices [38]. Based on the objectives of this study, the first scenario will be considered. According to Part II of Appendix C to Part 25 [37], the most critical ice accretion for airplane performance and handling qualities during each flight phase must be considered to demonstrate compliance with the relevant airplane performance and handling requirements in icing conditions. To reduce the number of ice accretions that need to be considered, the regulation allows for any of the specified ice accretions to be accepted if it is demonstrated to be more severe than the particular ice accretion defined for that phase of flight. Additionally, the most severe ice accretion in terms of its impact on handling qualities may be utilized for airplane performance tests, ensuring that any performance differences are conservatively considered. The latter is the main reason behind the common choice to estimate ice buildups on unprotected surfaces during a 45-minute holding condition. In this case, the Liquid Water Content (LWC) must be taken from the "continuous maximum" chart without any reduction, assuming the

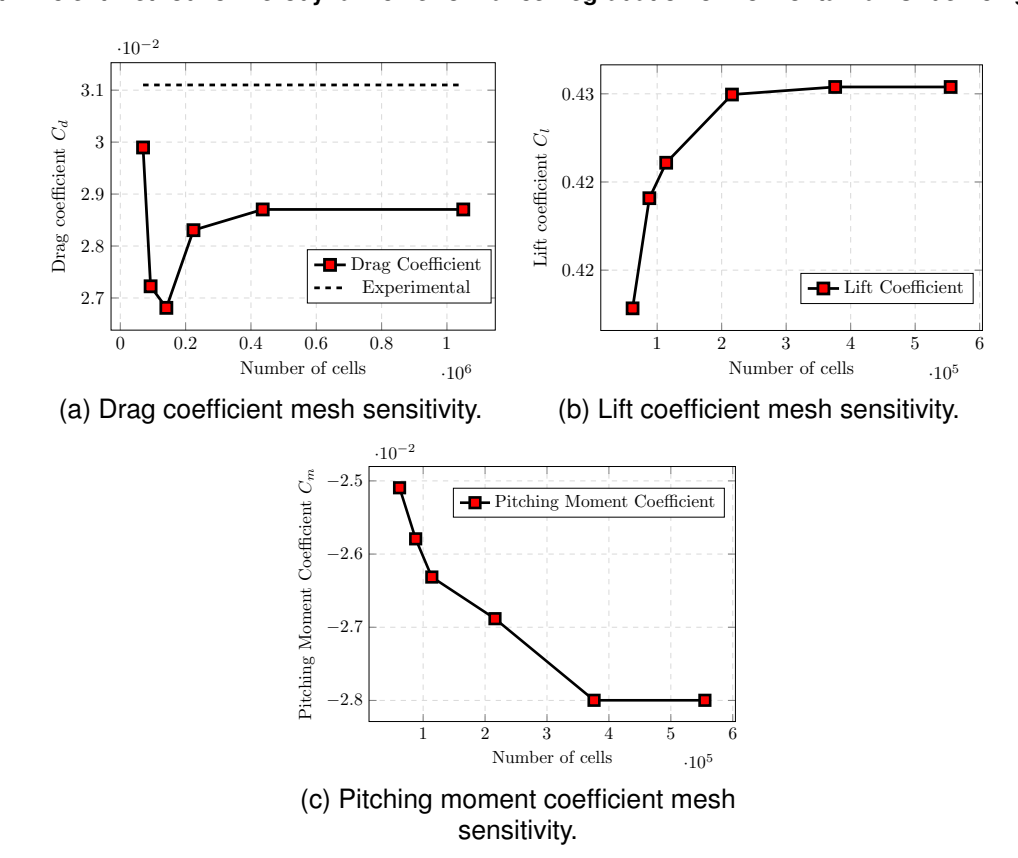


Figure 9 – Effect of mesh size on aerodynamics coefficients, NACA 0012, $V = 102.82 \,\mathrm{m/s}$, $\alpha = 4 \,\mathrm{deg}$.

Table 5 – Design of Experiments for the 2D aerodynamics.

Variable	Description	Lower Bound	Upper Bound
MVD (μm)	Mean Volume Diameter	15.0	40.0
T(K)	Temperature	243.15	273.15
M	Mach number	0.30	0.50
c (m)	Chord length	0.80	4.50
AoA_{ice} (°)	Angle of Attack for ice accretion	0.0	6.0

worst case scenario of a holding pattern occurring entirely within a region of cloudiness with the maximum probable LWC. Given the above, the sampling approach considered in this study aims to encompass the entire range of temperatures, liquid water contents, and droplet mean diameters specified by the "continuous maximum" as well as flight speeds and attitude angles as comprehensively as possible. To reduce the number of simulations required, a 45-minute holding situation has been deemed a sufficiently conservative scenario for assessing the impact of ice on aircraft tailplane aerodynamics.

According to the charts of Appendix C, the LWC values must be constrained by the limitations in terms of MVD and temperature. To introduce the constraints between the sampled variables, a Latin Hypercube Sampling with rejection has been implemented. The best compromise between the number of samples to be analyzed and the coverage of the LWC, MVD and Temperature chart has been achieved by having at least 100 samples laying within the prescribed chart limitations. A representation of the sampling performed in terms of the area covered of the continuous maximum exposure scenario of the Appendix C, is shown in Figure 10. Once the DoE has been generated, all the samples are processed to create the corresponding ice shapes and analyze their aerodynamic behavior through Computational Fluid Dynamics (CFD) simulations in both icing and non-icing conditions. All the aerodynamic curves have been collected and utilized to create a multidimensional database that serves as a 2D viscous data source for the 2.5D workflow. Specifically, this database encompasses

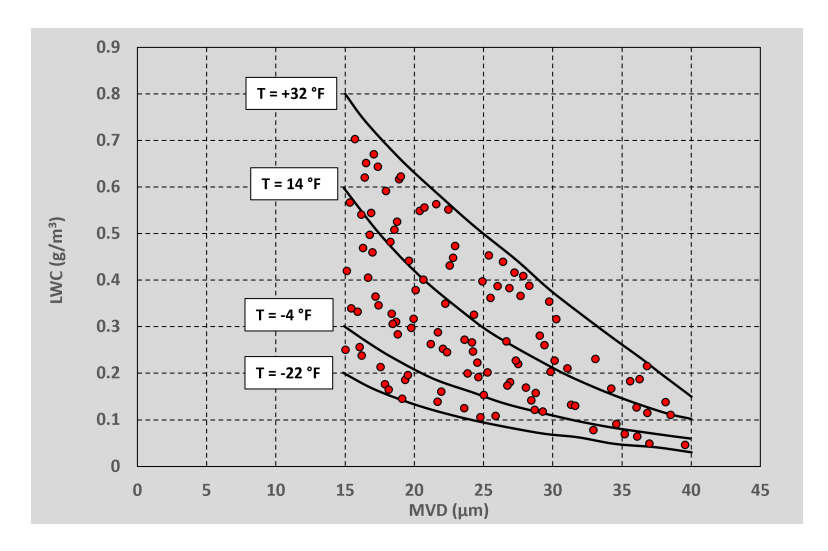


Figure 10 - Sampling of the Appendix C of 14 CFR Part 25 [37], continuous maximum scenario.

the key aerodynamic characteristics needed to reconstruct the curves of aerodynamic coefficients, such as:

- $C_{l_{max}}$, $C_{l_{\alpha}}$, α^{\star} , α_{stall} , C_{l_0} , $\alpha_{0,l}$;
- $C_{d_{min}}$, C_{l_i} , K;
- $C_{m_{ac}}$ and aerodynamic center coordinates (x_{ac}, y_{ac}) .

These coefficients are then used to generate:

• the lift curve for each section. This is achieved by considering a linear trend from $\alpha_{0,l}$ to α^* with a slope equal to $C_{l_{\alpha}}$ (3):

$$C_l(\alpha) = C_{l\alpha}(\alpha - \alpha_{0,l}) \quad \alpha_{0,l} \le \alpha \le \alpha^*$$
(3)

The non-linear trend is reconstructed using a quadratic Bezier curve (4):

$$\begin{cases}
\alpha(t) = (1-t)^2 \alpha^* + 2t(1-t)\alpha_1 + t^2 \alpha_{stall} & 0 \le t \le 1 \\
C_l(t) = (1-t)^2 C_l^* + 2t(1-t)C_{l_{max}} + t^2 C_{l_{max}} & 0 \le t \le 1
\end{cases}$$
(4)

where α_1 is given by (5):

$$\alpha_1 = \frac{C_{l_{max}} - C_{l,0}}{C_{l_{cc}}} \tag{5}$$

• the polar drag curve for each section. In this case, it is assumed that the curve is a parabola up until the point of stall (6):

$$C_d(C_l) = C_{d_{min}} + K(C_l - C_{l_i})^2 \quad C_{l,0} \le C_l \le C_{l_{max}}$$
(6)

• the pitching moment curve with respect to the chord quarter for each section can be determined by using (7):

$$C_m(\alpha) = C_{m_{ac}} - (x_{ac} - 0.25)(C_l \cos \alpha + C_d \sin \alpha) + -y_{ac}(C_l \sin \alpha - C_d \sin \alpha) \qquad \alpha_{0,l} \le \alpha \le \alpha_{stall}$$
(7)

Table 6 – 3D Experimental test cases conditions.

Variable	Description	Lower bound	Upper bound		
	Geometrical parameters				
R	Tailplane Aspect Ratio	4.0	6.0		
S	Tailplane area	$20.0{\rm m}^2$	$35.0\mathrm{m}^2$		
Λ_{le}	Leading edge sweep angle	$-20\deg$	30 deg		
λ	Taper ratio	0.25	0.80		
	lcing conditions				
\overline{M}	Mach number	0.30	0.50		
T	Temperature	243.15 K	273.15 K		
MVD	Water Droplet Median Volume Diameter	15.0 µm	40.0 µm		
$lpha_{\sf ice}$	Angle of attack for ice accretion	0 deg	6 deg		

3. Design of Experiments on a generalised 3D swept tailplane

Once the 2D aerodynamic databases have been generated, the proposed 2.5D approach was used to investigate a large number of potential jet aircraft tailplane configurations under various icing conditions. The aim is to generate sufficient information to develop a predictive method for ice-induced aerodynamic degradation using Response Surface Methodology (RSM). The latter could be exploited in preliminary aircraft design and optimization processes, unlocking the possibility of incorporating a complex and computationally costly discipline such as ice accretion.

In this study, in addition to the atmospheric icing conditions, a set of additional variables will be introduced to investigate a wide range of potential horizontal tailplane geometries.

The complete list of the exposed design variables and their lower and upper bounds is summarized in Table 6. To drastically cut the computational burden, the tailplane geometries investigated in this DoE will be provided with a single airfoil being the NACA 0009. This airfoil has been investigated under several icing conditions and chord lengths, as described in section 2.3.2

A design of experiments consisting of 1500 cases, encompassing 8 design variables (4 geometrical and 4 aerodynamic parameters) has been generated by means of Latin Hyper Cube sampling approach. It is worth remarking that the LWC is assumed as a function of T and droplets MVD to be compliant with the chart of Appendix C of 14 CFR Part 25 [37]. For each sampling point, all key aerodynamic characteristics and their relative variations between ice-off and ice-on have been extracted to reconstruct the tailplane aerodynamic coefficient curves. The stored information deals with the following aspects:

- Lift coefficient to reconstruct the zero-lift angle of attack α_{0l} , the lift coefficient at zero angle of attack C_{L0} , the lift curve slope $C_{L\alpha}$, the stall angle of attack α_{stall} , the maximum lift coefficient $C_{L,\max}$, the angle of attack at the end of linear range of lift α^* , and the corresponding lift coefficient C_L^* .
- Drag coefficient to estimate the penalty introduced by in terms of the minimum drag coefficient $C_{D_{\min}}$.
- Pitching moment coefficient to evaluate the impact the ice has on the pitching moment coefficient at zero lift C_{m_0} .

Response surfaces of degradation of all these aerodynamic characteristics due to ice have been developed as a function of the key geometrical and aerodynamic variables.

3.1 Ice-induced decay of aerodynamics coefficients

For the sake of brevity and clarity, this section will present the main results in terms of the impact of ice accumulation on the tailplane's lifting capabilities. This characteristic is crucial for determining

A Cost-Efficient Method for Aerodynamic Performance Degradation of Horizontal Tail Under Icing Conditions

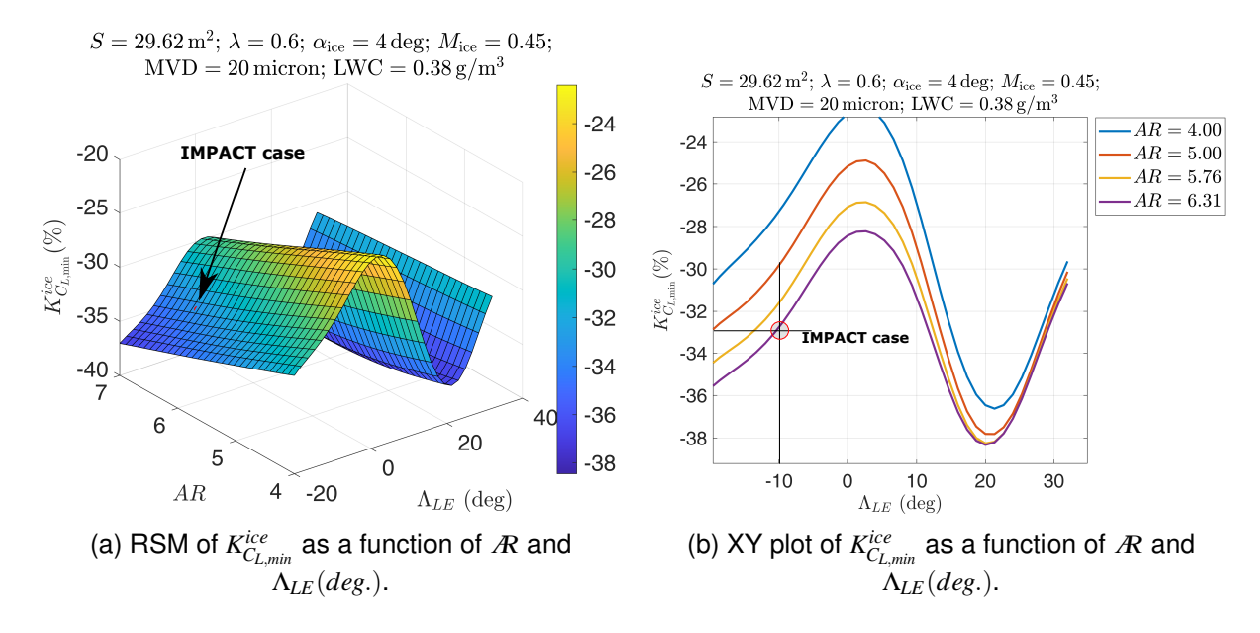


Figure 11 – Effect of tailplane sweep angle and \mathcal{R} on $K^{ice}_{C_{L,min}}$ under a fixed set of parameters: $S=29.62\,\mathrm{m}^2$; $\lambda=0.60$; $T_{ice}=261.15\,\mathrm{K}$; $\alpha_{ice}=4.0\,\mathrm{deg}$; $M_{ice}=0.45$; MVD = $20\,\mu\mathrm{m}$; LWC = $0.38\,\mathrm{g/m}^3$ according of the chart of Appendix C of 14 CFR Part 25, see Figure 10.

the size of the tailplane to ensure the stability and control of an airplane. Specifically, the following decays in terms of percentage reduction from ice-off and ice-on conditions will be shown:

- the maximum positive lift coefficient: $C_{L, \mathsf{max}}^{\mathsf{ice}} = \left(1 + K_{C_{L, \mathsf{max}}}^{\mathsf{ice}}\right) C_{L, \mathsf{max}}$
- the maximum negative lift coefficient: $C_{L, \mathsf{min}}^{\mathsf{ice}} = \left(1 + K_{C_{L, \mathsf{min}}}^{\mathsf{ice}}\right) C_{L, \mathsf{min}}$
- the lift curve slope: $C_{L\alpha}^{\text{ice}} = \left(1 + K_{C_{L\alpha}}^{\text{ice}}\right) C_{L\alpha}$

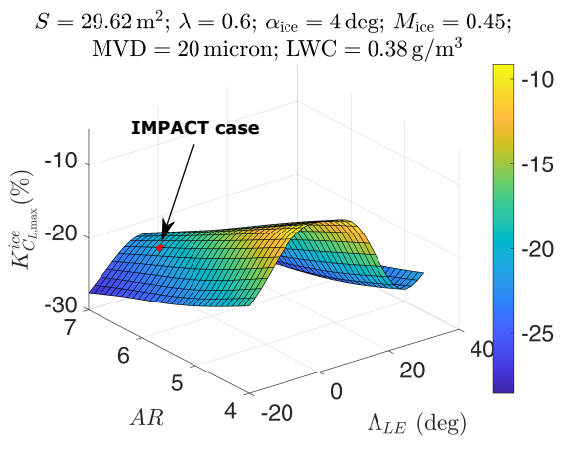
It must be highlighted that the developed Response Surface Models (RSM) have been prepared using the Radial Basis Function (RBF) methodology [39, 40]. This model can predict specific aerodynamic parameters based on a specified set of design variables and aerodynamic conditions.

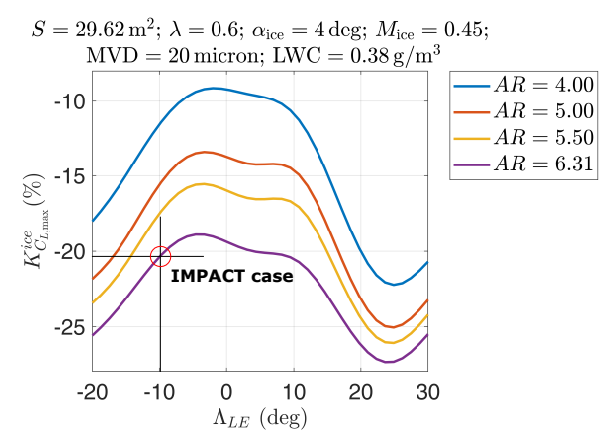
Response surface methodologies (RBFs) offer a flexible and effective approach to creating response surfaces, enabling the understanding and optimization of intricate relationships between input variables and output responses. This kind of model can be efficiently used to reduce the computational burden of Multi-Disciplinary Optimization tasks, as demonstrated by Lefebvre et al. [41].

The developed model can be easily integrated into an MDO workflow and queried by providing it with all the exposed design parameters, as described in section 3. A 3D representation of such kind of prediction models is shown in the chart of Figure 11, Figure 12 and Figure 13. The presented charts show a potential application of the proposed RSM models. The presented example depicts the effects of two geometrical characteristics of the tailplane, such as the sweep angle at the leading edge and the aspect ratio, under a fixed set of all other parameters. The atmospheric parameters have been set to the same conditions that were used to study the icing effects on a forward-swept tailplane as presented by Page et al. [22]. The point corresponding to the test case from Page et al. [22] is represented in the charts by a filled red dot. A comparison was made between the percentage variation in terms of the maximum negative lift coefficient and lift curve slope in the numerical results from Page et al. [22]. The results of the proposed Response Surface Methodology (RSM) based on the 2.5D approach presented here are shown in Table 7.

As can be appreciated by the comparison shown in Table 7, the results achieved by means of proposed approach are well aligned with the high-fidelity predictions.

A Cost-Efficient Method for Aerodynamic Performance Degradation of Horizontal Tail Under Icing Conditions





(a) RSM of $K_{C_{L,max}}^{ice}$ as a function of ${\cal R}$ and $\Lambda_{LE}(deg.)$.

(b) XY plot of $K_{C_{L,max}}^{ice}$ as a function of ${\cal R}$ and $\Lambda_{LE}(deg.)$.

-AR = 4.00

AR = 5.00

AR = 5.76

AR = 6.31

30

40

Figure 12 – Effect of tailplane sweep angle and \mathcal{R} on $K_{C_{L,max}}^{ice}$ under a fixed set of parameters: $\mathit{S} = 29.62\,\mathrm{m}^2;\,\lambda = 0.60;\,\mathit{T}_{\mathsf{ice}} = 261.15\,\mathrm{K};\\ \alpha_{\mathsf{ice}} = 4.0\,\mathrm{deg};\,\mathit{M}_{\mathsf{ice}} = 0.45;\,\mathsf{MVD} = 20\,\mu\mathrm{m};\,\mathsf{LWC} = 0.38\,\mathrm{g/m}^3$ according of the chart of Appendix C of 14 CFR Part 25, see Figure 10.

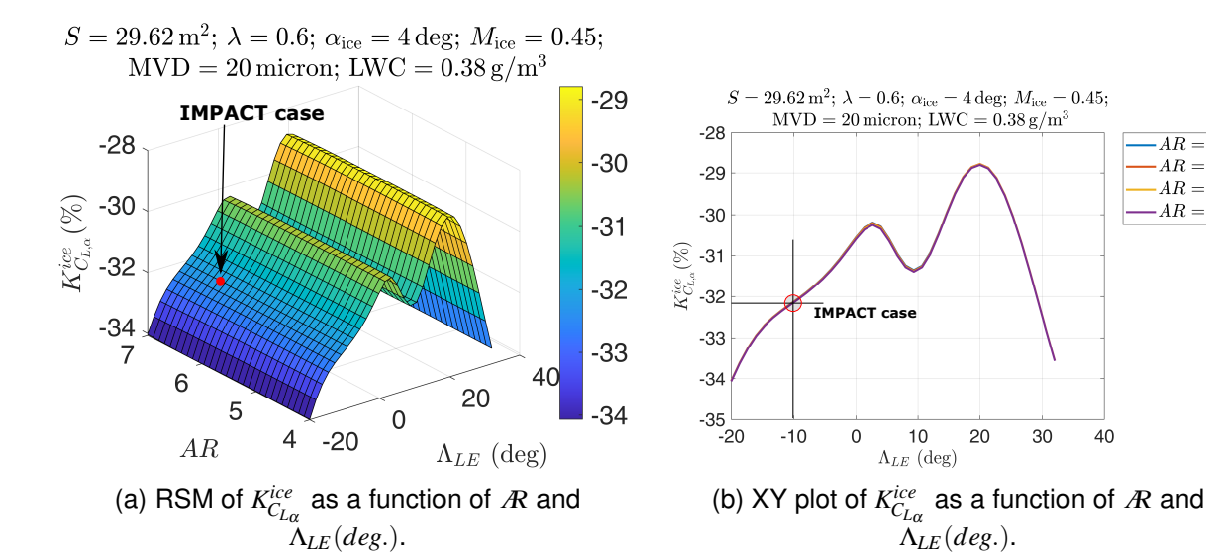


Figure 13 – Effect of tailplane sweep angle and R on $K_{C_{L_{\alpha}}}^{ice}$ under a fixed set of parameters: $S = 29.62 \,\mathrm{m}^2$; $\lambda = 0.60$; $T_{\text{ice}} = 261.15 \,\mathrm{K}$; $\alpha_{\text{ice}} = 4.0 \,\mathrm{deg}$; $M_{\text{ice}} = 0.45$; MVD = $20 \,\mu\mathrm{m}$; LWC = $0.38 \,\mathrm{g/m}^3$ according of the chart of Appendix C of 14 CFR Part 25, see Figure 10.

Table 7 - Comparison of percentage variation of aerodynamic coefficient between CFD results from Page et al. [22] and the proposed RSM model.

Coefficient	CFD	RSM
C_{Lmin} ICE-OFF	-0.6767	-0.512
C_{Lmin} ICE-ON	-0.4768	-0.346
$K_{C_{L_{min}}}^{ice}$	-29.53 (%)	-33.00 (%)
C_{Llpha} ICE-OFF	0.0586 (1/deg)	0.0529 (1/deg)
C_{Llpha} ICE-ON	0.0451 (1/deg)	0.0357 (1/deg)
$K_{C_{L_{\alpha}}}^{ice}(\%)$	-22.96 (%)	-32.05 (%)

Table 8 – Comparison of the computational costs between CFD from Page et al. [22] and the proposed approach.

RSM preparation			
Task	Nr. Of cases	Average Time per case (s)	Time (s)
2D Ice shape	100	5	500
2D CFD Ice-off	100	4000	400 000
2D CFD Ice-on	100	4620	462 000
2.5D Ice-Off	1500	36	54000
2.5D Ice-On	1500	45	67500
RBF Set-up	10	135	1350
ToT. (s)	-	-	985350
ToT. (days)	-	-	11
CFD analysis			
Task	Nr. Of cases	Average Time per case (s)	Time (s)
3D Ice shape	-	604800	604800
3D Ice-Off	-	86400	86400
3D Ice-On	-	604 800	604800
ToT. (s)	-	-	1296000
ToT. (days)	-	-	15

3.2 Computational cost analysis

The main objective of this work was to develop a fast yet reliable method to incorporate ice accretion considerations into aircraft Multi-Disciplinary Optimization workflows, with the goal of evaluating designs that are more tolerant to ice. This goal has been achieved by generating a large amount of data and organizing these databases into several response surfaces, which are essentially cost-effective in terms of computational expenses.

The computational cost of running a RSM model is practically zero; however, the data production required to train these models has a significant computational burden. It is worth comparing the time required for a complete high-fidelity ice accretion simulation and a sweep across several angles of attack to evaluate the aerodynamic behavior in ice-off and ice-on conditions, as well as the time needed to develop the RSM models and execute them. Data concerning the high-fidelity approach are extracted from Page et al. [22]. Table 8 presents a comprehensive comparison of the computational burden associated with the aforementioned approaches.

Data shown in Table 8 indicates that the time required to set up, run, and post-process a single case study using the most accurate numerical approach is comparable to the time needed to generate a large dataset for training a prediction method based on response surface methodology. It is clear that the proposed approach could be a viable solution to unlock the possibility of incorporating icing into complex Multidisciplinary Design Optimization (MDO) processes, where hundreds or even thousands of different aircraft designs need to be explored. The accuracy of the proposed approach has been revealed to be sufficient to provide reliable data regarding ice-induced aerodynamics, at least during the early aircraft design stages.

4. Conclusions

This paper introduced a tool that provides a cost-efficient approach to estimate the ice-induced aero-dynamic degradation of a generalized swept horizontal empennage. The feasibility of the proposed approach has been validated in terms of its capability to predict 2D ice shapes under various icing conditions and the reliability of the 3D prediction of the ice-induced decay of the lifting characteristics of a generalized swept tailplane. The developed approach has been proven to significantly reduce the time required to account for such a complex discipline. The proposed methodology is reliable enough to produce results comparable to the highest level of fidelity approaches, which are computa-

tionally expensive and prohibitive for introduction in complex multi-disciplinary optimization workflows aimed at aircraft optimizations. The proposed approach proved to be robust enough to predict the ice-induced deterioration in the empennage's aerodynamic performance. However, to account for all variables influencing the investigated phenomena, further analysis should be considered. The latter include the need to explore various airfoil shapes (e.g., modifying leading edge radius, thickness, camber, etc.), considering shadowing effects of other aircraft components like the wing and fuselage to account for changes in parameters affecting ice accretion, such as non-uniform liquid water content distributions, downwash, and local flow field variations. This field is a fertile domain to leverage the capabilities of Artificial Intelligence to explore, manage, and organize a wide range of data for a more comprehensive and robust approach in addressing such a complex discipline.

5. Contact Author Email Address

To contact mailto: salvatore.corcione@unina.it

6. Copyright Statement

The authors confirm that they, and/or their company or organization, hold copyright on all of the original material included in this paper. The authors also confirm that they have obtained permission, from the copyright holder of any third party material included in this paper, to publish it as part of their paper. The authors confirm that they give permission, or have obtained permission from the copyright holder of this paper, for the publication and distribution of this paper as part of the ICAS proceedings or as individual off-prints from the proceedings.

References

- [1] Reehorst A, Chung J, Potapczuk M and Choo Y. Aircraft flight characteristics in icing conditions. *Journal of Aircraft*, Vol. 37, No 2, pp 253-259, 2000.
- [2] Cao Y, Wu Z, Su Y and Xu Z. Aircraft flight characteristics in icing conditions. *Progress in Aerospace Sciences*, Vol. 74, pp 62-80, 2015.
- [3] Cole J and Sand W Statistical study of aircraft icing accidents. *AIAA 29th Aerospace Sciences Meeting*, Reno, NV, Jan. 7-10, 1991, 1991-0117, 1991.
- [4] Gent R.W, Dart N.P and Cansdale J.T. Aircraft icing. *Philosophical Transactions of the Royal Society of London A: Mathematical, Physical and Engineering Sciences*, Vol. 358, No 1776, pp 2873-2911, 2000.
- [5] Bragg M.B. Rime ice accretion and its effect on airfoil performance. *National Aeronautics and Space Administration*, NASA Contractor Report 165599, Lewis Research Center, 1982.
- [6] Addy H.E, Potapczuk M.G and Sheldon M.G. Modern airfoil ice accretions. *35th Aerospace Sciences Meeting and Exhibit*, Reno, Nevada, January 6-10, AIAA Paper 97-0174, 1997.
- [7] Shin J and Bond T.H. Results of an icing test on a NACA 0012 airfoil in the NASA Lewis Icing Research Tunnel. *30th Aerospace Sciences Meeting and Exhibit*, Reno, Nevada, January 6-9, AIAA PAPER 92-0647, 1992.
- [8] Shin J. and Bond T.H. Experimental and computational ice shapes and resulting drag increase for a NACA 0012 airfoil. Symposium on Numerical and Physical Aspects of Aerodynamic Flows, Long Beach, CA, United States, January 13-16, 1992.
- [9] National Transportation Safety Board. In-Flight Icing encounter and Loss of Control Simmons Airlines, d.b.a. American Eagle Flight 4184, Avions de Transport Regional (ATR) model 72-212. National Aeronautics and Space Administration, NTSB, U.S. National Transportation Safety Board, N401AM, Roselawn, Indiana October 31, 1994.
- [10] Wilder R.W. A theoretical and experimental means to predict ice accretion shapes for evaluating aircraft handling and performance characteristics. *AGARD Aircraft Icing (SEEN 79-15036 06-05)*, 1978.
- [11] Bidwell C.S and Potapczuk M.G. User's Manual for the NASA Lewis Three-Dimensional Ice Accretion Code (LEWICE3D). *National Aeronautics and Space Administration*, NASA-TM-105974, 1993.
- [12] Beaugendre H, Morency F and Habashi W.G. Development of a Second Generation In-Flight Icing Simulation Code. *Journal of Fluids Engineering*, Vol. 128, No 2, pp 378-387, 2005.
- [13] Hasanzadeh K, Laurendeau E and Paraschivoiu I. Quasi-steady convergence of multistep Navier–Stokes icing simulations. *Journal of Aircraft*, Vol. 50, No 4, pp 1261-1274, 2013.
- [14] Montreuil E, Chazottes A, Guffond A, Murrone A, Caminade F and Catris S. ECLIPPS: 1. Three Dimensional CFD Prediction of the Ice Accretion. *1st AIAA Atmospheric and Space Environments Conference*, San Antonio, Texas, June 22-25, 2009.

- [15] Li S, Qin J, He M and Paoli R. Fast Evaluation of Aircraft Icing Severity Using Machine Learning Based on XGBoost. *Aerospace*, Vol. 7, No 4, pp 364, 2020.
- [16] Jung S, Myong R and Cho T. Efficient Prediction of Ice Shapes in CFD Simulation of In-flight Icing Using a POD-Based Reduced Order Model. *SAE International Journal of Aerospace*, Vol. 4, No 1, pp 1-10, 2011.
- [17] Kang Y.E and Yee K. Efficient Prediction of Ice Shapes in CFD Simulation of In-flight Icing Using a POD-Based Reduced Order Model. *Journal of the Korean Society for Aeronautical and Space Sciences*, Vol. 50, No 3, pp 147-155, 2022.
- [18] Han Y and Palacios J. Validation of a LEWICE-based Icing Code with Coupled Heat Transfer Prediction and Aerodynamics Performance Determination. 9th AIAA Atmospheric and Space Environments Conference, Denver, Colorado, June 5-9, 2017.
- [19] Jeck R.K. Icing Design Envelopes (14 CFR Parts 25 and 29, Appendix C) Converted to a Distance-Based Format. *Federal Aviation Administration*, Report No DOT/FAA/AR-00/30, 2002.
- [20] Miller D.R, Addy H.E and Ide R.F. A study of large droplet ice accretions in the NASA Lewis IRT at near-freezing conditions. 34th Aerospace Sciences Meeting and Exhibit, Reno,NV,U.S.A., January 15-18, 1996.
- [21] Bragg M.B and Loth E. Effects of Large-Droplet Ice Accretion on Airfoil and Wing Aerodynamics and Control. *Federal Aviation Administration*, Report No DOT/FAA/AR-00/14, 2000.
- [22] Page J, Ozcer I, Zanon A and De Gennaro M. IMPACT: Numerical Study of Aerodynamics of an Iced Forward-Swept Tail with Leading Edge Extension. *SAE Technical Paper*, 2023-01-1371, 2023.
- [23] Fujiwara G.E and Bragg M.B. 3D computational icing method for aircraft conceptual design. *9th AIAA Atmospheric and Space Environments Conference*, Denver, Colorado, June 5-9, 2017.
- [24] Hedde A.T and Guffond A.D. Improvement of the ONERA 3D icing code, comparison with 3D experimental shapes. 31st Aerospace Sciences Meeting, Reno, NV, U.S.A., January 11-14, 1993.
- [25] Kays W.M, Crawford M.E and Weigand B. *Convective Heat and Mass Transfer*. 1st edition, Tata McGraw-Hill Education, 2012.
- [26] Messinger B.L. Equilibrium Temperature of an Unheated Icing Surface as a Function of Air Speed. *Journal of the Aeronautical Sciences*, Vol. 20, No 12, pp 849-850, 1953.
- [27] Makkonen L. Heat transfer and icing of a rough cylinder. Cold Regions Science and Technology, Vol. 10, No 2, pp 105-116, 1985.
- [28] Shin J, Berkowitz B, Hsun C and Cebeci T. Prediction of ice shapes and their effect on airfoil performance. *29th Aerospace Sciences Meeting*, Reno, NV, U.S.A., January 7-10, 1991.
- [29] Laurendeau E, Bourgault-Cote S, Ozcer I, Hann R, Radenac E and Pueyo A. Summary from the 1st AIAA Ice Prediction Workshop. *AIAA AVIATION 2022 Forum*, Chicago, IL, Virtual, June 27 July 1, 2022.
- [30] Goitia H and Llamas Sandin R. Nonlinear vortex lattice method for stall prediction. *9th EASN International Conference on "Innovation in Aviation and Space*, Athens, Greece, September 3-6, 2019.
- [31] Della Vecchia P, Nicolosi F, Ruocco M and De Marco A. An improved high-lift aerodynamic prediction method for transport aircraft. *CEAS Aeronautical Journal*, Vol. 10, No 3, pp 795-804, 2019.
- [32] Shin J and Bond T.H. Experimental and computational ice shapes and resulting drag increase for a NACA 0012 airfoil. *Symposium on Numerical and Physical Aspects of Aerodynamic Flows*, Long Beach, CA, U.S.A., January 13-16, 1992.
- [33] Shaw R.J and Potapczuk M.G. Predictions of Airfoil Aerodynamic Performance Degradation Due to Icing. Fourth Symposium on Numerical and Physical Aspects of Aerodynamic Flows, Long Beach, CA, U.S.A., January 16-19, 1989.
- [34] Tang B. Orthogonal array-based Latin hypercubes. *Journal of the American statistical association*, Vol. 88, No 424, pp 1392-1397, 1993.
- [35] Owen A.B. Orthogonal Arrays for Computer Experiments, Integration and Visualization. *Journal of the American Statistical Association*, Vol. 93, No 444, pp 1430-1439, 1998.
- [36] Ye K.Q. Orthogonal column Latin hypercubes and their application in computer experiments. *Statistica Sinica*, Vol. 2, No 2, pp 439-542, 1992.
- [37] Federal Aviation Regulation. Appendix C to Part 25 Atmospheric Icing Conditions. 14 CFR Appendix C to Part 25 Appendix C to Part 25, February 16, 2024.
- [38] Jeck R.K. Icing Design Envelopes (14 CFR Parts 25 and 29, Appendix C) Converted to a Distance-Based Format. *Federal Aviation Administration Technical Center Atlantic City NJ*, DOT/FAA/AR-00/30, Washington, D.C., 20591, April, 2002.
- [39] Dash C.S.K, Behera A.K, Dehuri S and Cho S.B. Radial basis function neural networks: a topical state-of-the-art survey. *Open Computer Science*, Vol. 6, No 1, pp 33-63, 2016.

A Cost-Efficient Method for Aerodynamic Performance Degradation of Horizontal Tail Under Icing Conditions

- [40] Lee C.C, Chung P.C, Tsai J.R and Chang C.I. Robust radial basis function neural networks. *IEEE Transactions on Systems, Man, and Cybernetics, Part B (Cybernetics)*, Vol. 29, No 6, pp 674-685, 1999.
- [41] Lefebvre T, Bartoli N, Dubreuil S, Panzeri M, Lombardi R, Della Vecchia P, Stingo L, Nicolosi F, De Marco A, Ciampa P, Anisimov K, Savelyev A, Mirzoya A and Isyanov A. c. *Progress in Aerospace Sciences*, Vol. 119, pp 0376-0421, 2020.